
SEMI- ANALYTICAL BENCHMARKS
for
STEADY STATE NEUTRON TRANSPORT
in
INFINITE MEDIA
for
SELECTED SOURCES

Joint Benchmark Committee
sponsored by
Mathematics and Computation, Radiation Protection and Shielding, and Reactor Physics Divisions
of the
American Nuclear Society

Developed and Distributed
by

B. Ganapol
Mathematics and Computation Division
American Nuclear Society

Contact Information:
Barry D. Ganapol
Department of Aerospace and Mechanical Engineering
Rm. 727 AME Bldg.
1130 N. Mountain Ave.
University of Arizona
Tucson AZ 85721
Tel: 520/621-4728
Ganapol@cowboy.ame.arizona.edu

TABLE of CONTENTS

Tables:

Figures:

1. INTRODUCTION

The design of nuclear power reactors including safety analyses and burnup predictions are commonplace in today's large-scale computational environment. Methods developers have perfected computational algorithms for cross section generation, neutron transport and diffusion calculations, and Monte Carlo simulations in order to take advantage of emerging computational architectures and strategies. As computational capacity increases with improvement in microchip efficiency according to Moore's law, we can accommodate ever-larger reactor calculations. Along with these advances in large-scale computing has come an increased reliance on numerical methods and, as a result, the development of more powerful and sophisticated numerical algorithms. In particular, finite difference, finite element, finite volume, nodal, P_N and S_N methods are among today's most effective numerical algorithms for neutron transport theory applications. While these methods allow for consideration of comprehensive problems in reactor physics, they all generally possess one inherent shortcoming, i.e., numerical discretization error. This error results from the finiteness, though large by past standards, of computer storage. Of course, for many algorithms, an estimate of the numerical error usually provides only an approximate upper bound and can, under certain circumstances, be quite misleading. In addition, because of the mathematical and numerical complexity of current schemes, proper programming of a neutron transport algorithm becomes an issue.

In these times of accountability and continuous improvement, it is imperative that code users are confident of acceptable numerical error and proper programming. To assess numerical error of a particular algorithm and its proper programming, verification, including one or all of the following tests, has routinely been a part of the code development process:

1. Monitoring conservation of quantities such as particle number, total energy and momentum
2. Comparisons to known physical trends usually involving simplified problems with predictive behavior
3. Comparisons to algorithms designed for similar applications
4. Construction of manufactured solutions
5. Comparisons to standards or analytical or semi- analytical benchmarks

It must be emphasized that there is no guaranteed method of verifying that a particular computational algorithm performs correctly for all cases envisioned since, if there were, there would be no need for the algorithm in the first place. The value of the tests mentioned above is in indicating algorithmic inconsistencies by their failure. Note that comparison to experiment is not included as one of the tests considered, since comparison to experiment measures how well one models a particular physical situation indicating nothing about the quality of the numerical results. For this reason, comparison to experiment is a code *validation* measure rather than a code *verification* measure as afforded by analytical or semi- analytical benchmarks.

The primary aim of this semi- analytical benchmark presentation is to provide a series of analytical benchmarks or standards of comparison. Currently, there is a lack of such benchmarks in the literature; and it is for this reason, that this series has relevance. A secondary use of these benchmarks derives from their educational value. To generate a benchmark requires a firm grasp of analytical solution techniques as well as numerical methods and computational strategies. For curricula in nuclear engineering, the introduction of theory of analytical benchmarks enhances the concepts of neutron interaction with matter. In addition, the subject of analytical benchmarking introduces the student to standard numerical techniques such as numerical integration and iteration as well as analytical mathematical methods, appropriate computational strategies and error analysis.

2. OVERVIEW OF ANALYTICAL BENCHMARKING

2.1 Hierarchy of Analytical Benchmarks

When solving the neutron transport equation, a hierarchy of analytical solutions, based on accuracy and precision, is possible. In the context used here, we primarily are assessing precision since we seldom have the exact solution for comparison.

The hierarchy is as follows:

- ❑ exact- analytical
- ❑ near- analytical
- ❑ semi- analytical
- ❑ purely- numerical.

A closed form *exact- analytical* numerical solution is the ideal solution one strives toward when numerically solving any equation. In this case, an explicit closed form solution representation exists in terms of elementary functions. The most precise numerical evaluation of this form therefore is through infinite precision arithmetic, thus avoiding truncation error altogether. Unfortunately, the solutions to particle transport equations do not lend themselves to simple closed form representations. With the increased use of symbolic manipulation for numerical evaluation however, the ideal of the *exact- analytical* solution will most likely become possible in the near future. A *near- analytical* solution to the transport equation is an evaluation of a closed form solution representation using standard numerical approximations with high-precision arithmetic. Such an evaluation may make use of numerical quadrature and infinite series for which error estimates are available. *Semi- analytical* solutions are finite precision numerical evaluations of a continuous variable solution representation, which, for example, may be in the form of a set of integral equations. These solutions generally require iterative techniques with inherent error control and the potential for acceleration toward convergence to the exact solution. Examples of *semi- analytical* solutions are derived from integral transport theory and the 1-D Green's Function Method [Ganapol,1999b]. Finally, the most common solutions to the transport equation involve full numerical discretization of the transport operator with respect to particle position, direction, time and energy. *Purely numerical* solutions, while containing discretization error, are nevertheless, the most comprehensive transport solutions available and are the foundation of numerical transport applications. Algorithms such as discrete ordinates (also called the SN formulation) can generate ultra-fine mesh benchmark solutions that are as precise as semi- analytical benchmarks [Ganapol,1999a].

There are several important distinctions between "semi- analytical" and "purely- numerical" solutions. First, like numerical solutions, semi-analytical benchmarks contain unavoidable numerical error resulting from finite precision arithmetic and numerical approximation. Unlike purely

numerical solutions, however, one can estimate the error associated with semi- analytical benchmarks, which occurs at a level theoretically close to the true analytical solution. For this reason, semi- analytical benchmarks represented the highest standard of quality we could achieve until recently. This has changed with convergence acceleration however, unfortunately not considered in this benchmark series.

In general, benchmarks can effectively uncover unknown numerical vagaries and coding errors, to assess the precision of purely numerical transport algorithms as well as to confirm proper algorithm performance. The series of semi- analytical infinite medium benchmarks presented here will serve as convenient standards to compare to numerical neutron transport algorithms. This is not to say that fine mesh numerical benchmarks cannot be as precise as analytical benchmarks (especially with convergence acceleration), but ultimate confidence in their precision only comes with comparison to semi-analytical benchmarks.

Because of the requirement of analytical representations, we only consider relatively simple or idealized problems for semi- analytical benchmarks. For this reason, semi- analytical benchmarks have the potential to verify only isolated segments of large comprehensive algorithms. Through verification of components of an algorithm, one does gain some confidence in the operation of a code. Inconsistencies and inaccuracies may remain however because of the interfacing of components. It must be emphasized that even though the type of problems lending themselves to analytical solution representation are usually considerably less sophisticated than the comprehensive problems for which a code has originally been designed, they still have significant diagnostic value. Indeed, codes required to solve the comprehensive problems must also perform well for the simple ones.

2.2 Benchmark Classification

Since many benchmarks are possible, a convenient classification scheme provides a reference, with each benchmark classified according to the eight categories shown in Table A.

The first category (*C1*) specifies the type of particle considered which include neutrons, photons, electrons, ions and molecules. In future efforts,

Table A. Benchmark Classification.

C1. SPECIFIC TRANSPORT FIELD	
NT	Neutron transport
ND	Neutron diffusion
RT	Radiative transfer
EIT	Electron and ion transport
RGD	Rarefied gas dynamics

C2. GEOMETRY		
P	Plane geometry	(1D,2D)
SP	Spherical geometry	(1D)
CY	Cylindrical geometry	(1D,2D)
I	Infinite Medium	

SPECIFIC GEOMETRY QUALIFIERS	
I	Infinite medium
H	Half-space
2H	2 Half-spaces
S	Slab geometry
HE	Heterogeneous slab geometry

C3. ANISOTROPY OF SCATTERING KERNEL	
I	Isotropic
LE(*L*)	Legendre expansion of order *L*

C4. ENERGY SPECTRUM APPROXIMATION	
OG	One-group
MG	Multigroup
C	Continuous

C5. ANGULAR SOURCE DISTRIBUTION	
I	Isotropic
B	Beam
D	Distributed
LE(*L*)	Legendre expansion of order *L*

C6. SPATIAL AND/OR TEMPORAL SOURCE DISTRIBUTION	
L	Localized (delta function)
D	Distributed
PT	Pulsed in time
CT	Continuous in time
U	Uniform Spatially

C7. NUMERICAL TREATMENT OF INDEPENDENT VARIABLES		
X(C,D)	Position	(continuous, discrete)
A(C,D)	Angle	(continuous, discrete)
T(C,D)	Time	(continuous, discrete)
E(C,D)	Energy	(continuous, discrete)

C8. NUMERICAL METHOD	
NLTI	Numerical Laplace transform inversion
NFTI	Numerical Fourier transform inversion
FN	FN method
IT	Integral transport
VM	Variational method
RM	Reconstruction from moments
MC	Multiple collision
RR	Recurrence relation
CAC	Continuous analytical continuation
EE	Eigenfunction expansion
Other	PN, AN, etc.

the benchmark suite could be expanded to include all the particle transport theories indicated in *C1*. Here, we consider only neutrons. Category 2 (*C2*) specifies the geometry containing the field particles with which the neutrons collide, with one- and two- infinite medium benchmarks considered. In general, the geometry can be infinite without surfaces, 1D or 2D half-spaces with one surface and a 1D finite media with two surfaces. These geometries comprise a future effort. *C3* specifies the type of scattering kernel (isotropic, anisotropic, or general) with the neutron energy spectrum approximation (one-group, multigroup, or continuous) given in *C4*. We consider only one-group benchmarks here. *C5* and *C6* give the angular and spatial source distributions respectively. Information on the numerical method is given in *C7* and *C8*, indicating which independent variables are treated either continuously (C) or discretely (D) in *C7* and the particular numerical method used in *C8*.

3. INFINITE MEDIUM BENCHMARKS

3.1. General Physical Description

The most fundamental spatial configuration for the transport of neutrons is the infinite homogeneous medium. While conceptually, the infinite medium calls up a rather overwhelming image of a large universe that is primarily of mathematical interest only, a closer look reveals a structure that can be useful in generating meaningful analytical transport numerical standards. An infinite medium comes in many flavors as defined by the configuration of the source. For instance, if the source is an infinitesimally thin and transversely infinite plane (1D Plane), the variation of the resulting flux is longitudinal only (say in the x-direction). This is true since no surfaces or material discontinuities exist to influence particles otherwise. If the source is a point and is isotropically emitting in the same infinite medium, then the flow is radially outward giving rise to the well-known inverse r-squared flux behavior. A vertically infinite isotropically emitting line source exhibits an axially uniform radial flow. Of course, the main reason for these simple variations is that a homogeneous infinite medium has no distinguishing characteristics such as surfaces or material boundaries (other than a source position) to define a length scale. For this reason, the dimensional variation of the flux in an infinite medium inherits the dimensionality of the source. The flux from a plane source therefore only has variation in the longitudinal spatial dimension; while, the flux for an isotropically emitting point source is uniformly distributed on spherical surfaces. With this in mind, it is possible to define several relatively simple source configurations to provide multi-dimensional flux variation. This observation along with the analytical relations between fluxes in infinite media, allow for the development of a convenient tool to generate some rather comprehensive multidimensional analytical benchmark solutions in anisotropically scattering media. The generation of four simple 1D and two 2D benchmark solutions follows.

3.2. The Sources

3.2.1 Plane Source: NT/P: I/LE/OG/I/L/X(C), A(C)/NFTI

Description:

A plane source emits isotropically in an infinite medium at x=0. The medium

scatters anisotropically to any finite degree of Legendre expansion L of the scattering kernel. Because of symmetry, edits of the scalar flux are at only positive positions (measured in mean free paths) from the source.

Theory

The theory begins with the solution of the following one-group transport equation:

$$\left[\mu\frac{\partial}{\partial x}+1\right]\Psi(x,\mu)=\frac{c}{2}\sum_{l=0}^{L}\omega_l P_l(\mu)\Psi_l(x)+\frac{\delta(x)}{2}. \qquad (1)$$

$\Psi(x,\mu)$ represents the angular flux distribution of particles traveling in the direction μ (with respect to the x-axis) at the position x (measured in mean free paths from the source plane) and emitted isotropically by a source at x = 0. The solution emerges after application of the following Fourier transform inversion **(**See **APPENDIX A** [Eq. (A12)]):

$$\Psi(x)\equiv\frac{1}{2\pi}\int_{-\infty}^{\infty}dk\ e^{ikx}\left[\frac{\tilde{g}_L(k)}{\Lambda_L(k)}\right]. \qquad (A12)$$

The inversion, performed numerically, appears in **APPENDIX C**.

Sample Problems 1 and 2

In this problem, we investigate convergence with requested error. We consider a homogeneous infinite medium with a Henyey-Greenstein (H-G) scattering kernel ($\omega_l \equiv g^l$) of average cosine g = 0.9 and number of secondaries c = 0.9. The order of the scattering approximation is fixed at L = 12. To demonstrate benchmark precision, Table 1 shows four cases of decreasing requested relative errors of 10^{-3}, 10^{-5}, 10^{-7} and 10^{-9}. We observe convergence with decreasing error to five places.

Table 1. Sample Problem 1: Plane Source Convergence with Error

x/ε	10^{-3}	10^{-5}	10^{-7}	10^{-9}
1.00000E-02	3.29089E+00	3.29086E+00	3.29086E+00	3.29086E+00
1.12000E+00	9.44994E-01	9.45000E-01	9.45001E-01	9.45001E-01
2.23000E+00	6.26033E-01	6.26039E-01	6.26039E-01	6.26039E-01
3.34000E+00	4.52284E-01	4.52290E-01	4.52290E-01	4.52290E-01
4.45000E+00	3.39081E-01	3.39088E-01	3.39088E-01	3.39088E-01
5.56000E+00	2.59366E-01	2.59365E-01	2.59365E-01	2.59365E-01
6.67000E+00	2.00814E-01	2.00813E-01	2.00813E-01	2.00813E-01
7.78000E+00	1.56710E-01	1.56709E-01	1.56709E-01	1.56709E-01
8.89000E+00	1.22946E-01	1.22945E-01	1.22945E-01	1.22945E-01
1.00000E+01	9.68140E-02	9.68134E-02	9.68134E-02	9.68134E-02

Sample Problem 2 graphically illustrates the convergence of the scattering kernel with respect to scattering order L. For a H-G kernel with average cosine of g = 0.99, representing an extremely forward peaked scattering kernel, and c = 0.9, Fig. 1 shows the convergence in scattering order for L = 0, 2, 4, 6, 12, 24. For forward peaked scattering, depletion of neutrons near

Fig. 1. Sample Problem 2: Plane Source--Variation of L

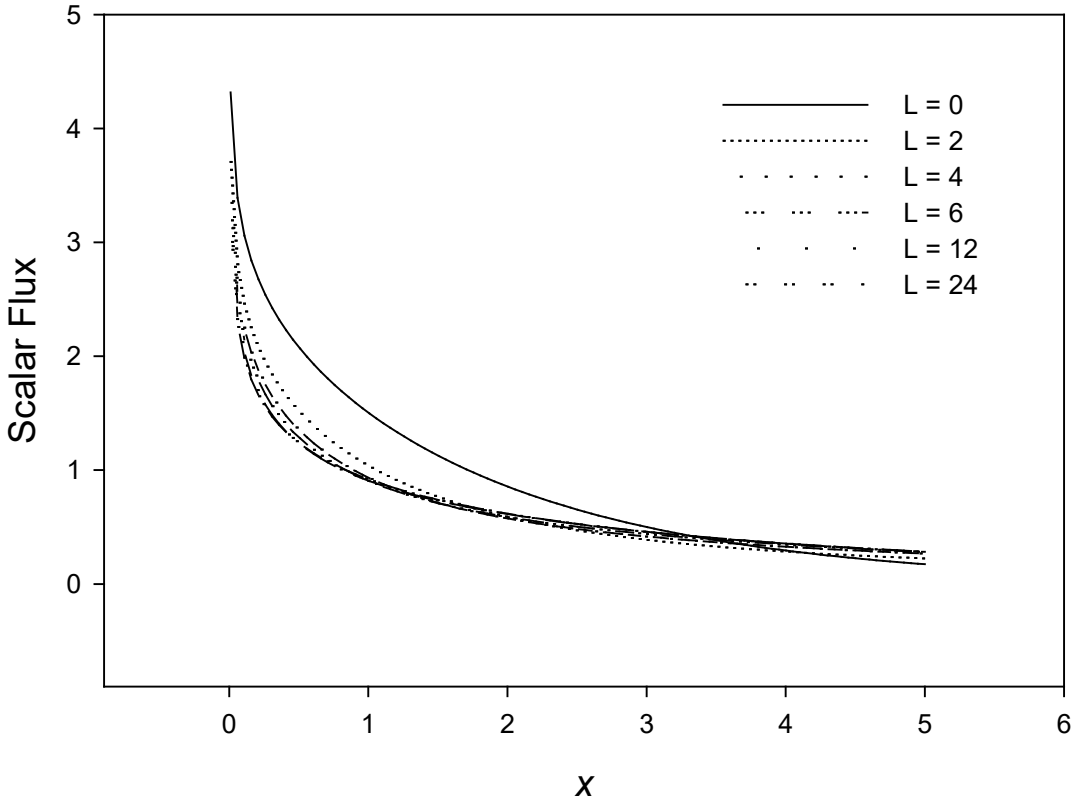

the source occurs as they transport further into the medium more readily than for isotropic scatter.

3.2.2. Point Source: NT/SP: I/LE/OG/I/L/X(C), A(C)/NFTI

With explicit representation of the scalar flux in a plane infinite medium known, it is now possible to define flux variations for sources in other more complex and realistic infinite media settings.

Description

A point source, at $r = 0$, emits isotropically in an anisotropically scattering infinite medium. Edits of the scalar flux at radial distances (measured in mean free paths) from the source are recorded.

Theory

The flux from a point source comes from the plane/point transformation [Case,1967]

$$\Phi_{pt}(r) = -\frac{1}{2\pi r}\frac{d\Psi(r)}{dr}, \tag{2}$$

which gives from Eq(A12)

$$\Phi_{pt}(r) \equiv \frac{1}{2\pi}\int_{-\infty}^{\infty} dk\; e^{ikr}\left[\frac{\tilde{g}_L(k)}{z\Lambda_L(k)}\right]. \tag{3}$$

Sample Problems 3 and 4

Sample Problem 3 for the point source considers the same medium as Sample Problem 1. Table 2 shows the results similarly indicating convergence.

Table 2. Sample Problem 3: Point Source Convergence with Error

r/ε	10^{-3}	10^{-5}	10^{-7}	10^{-9}
1.00000E-02	7.97811E+02	7.97810E+02	7.97810E+02	7.97810E+02
1.12000E+00	6.03746E-02	6.03746E-02	6.03746E-02	6.03746E-02
2.23000E+00	1.42703E-02	1.42703E-02	1.42703E-02	1.42703E-02
3.34000E+00	5.87232E-03	5.87221E-03	5.87221E-03	5.87221E-03
4.45000E+00	3.01848E-03	3.01838E-03	3.01839E-03	3.01839E-03
5.56000E+00	1.74585E-03	1.74586E-03	1.74586E-03	1.74586E-03
6.67000E+00	1.08519E-03	1.08520E-03	1.08520E-03	1.08520E-03
7.78000E+00	7.07543E-04	7.07548E-04	7.07548E-04	7.07548E-04
8.89000E+00	4.77065E-04	4.77068E-04	4.77068E-04	4.77068E-04
1.00000E+01	3.29671E-04	3.29673E-04	3.29673E-04	3.29673E-04

Sample Problem 4 considers a variation of c with results shown in Fig. 2. Asymptotic exponential behavior is evident at large distances from the source.

Fig. 2.Sample Problem 4: Point Source-Variation of c

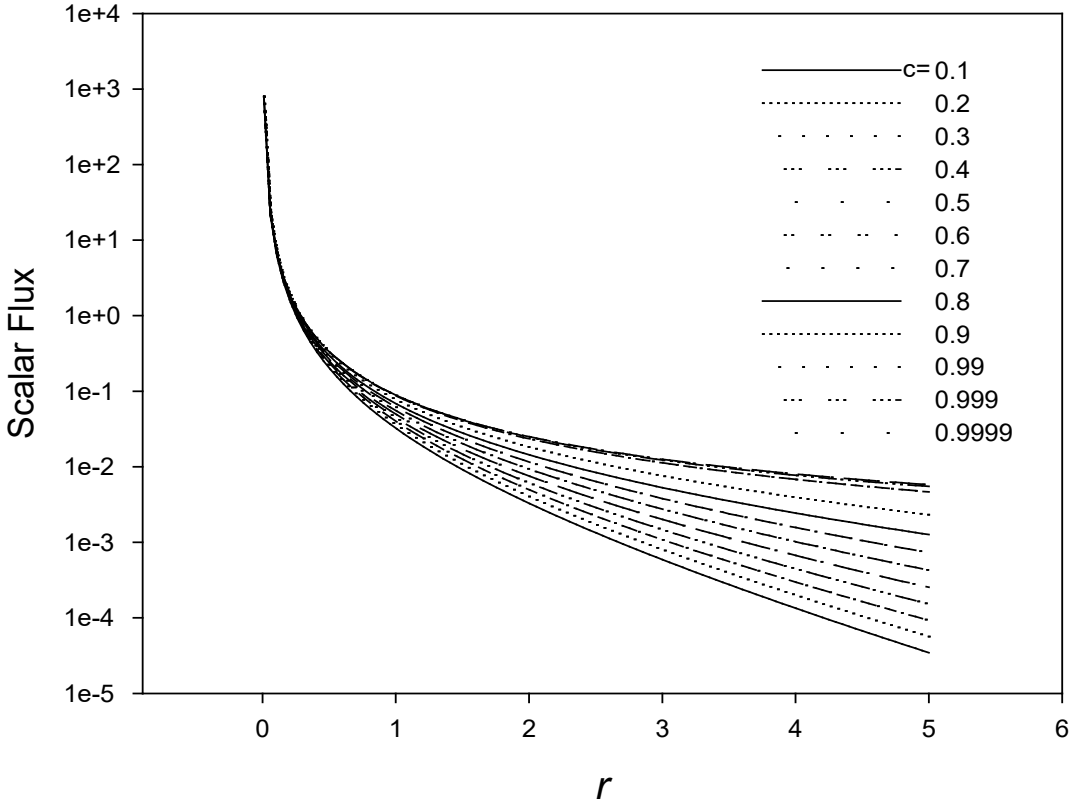

3.2.3. Shell Source: NT/SP: I/LE/OG/I/L/X(C), A(C)/NFTI

Description

For this case, an infinitesimally thin shell source of radius *a* isotropically emits in an infinite medium.

Theory

The point source flux then gives the flux from a shell source of radius *a*. If one integrates a point source over the shell of as shown, the flux at *r* is

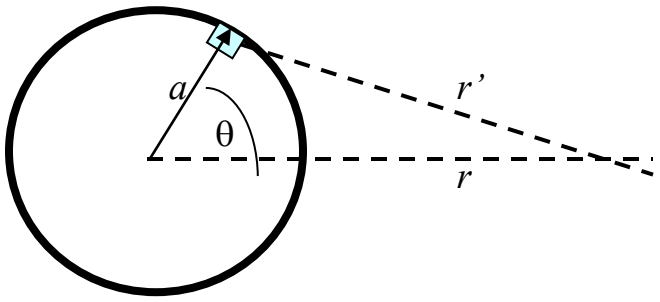

$$\Phi_{sh}(r,a) = q_0 \frac{a}{r}\left[\Phi_{pl}(|r-a|) - \Phi_{pl}(r+a)\right]. \quad (4a)$$

For a normalization of one particle emitted over the entire shell area

$$q_0 = \frac{1}{4\pi a^2}, \quad (4b)$$

we have

$$\Phi_{sh}(r,a) = \frac{1}{4\pi a r}\left[\Phi_{pl}(|r-a|) - \Phi_{pl}(r+a)\right]. \quad (5)$$

Sample Problem 5

Table 3. Sample Problem 5: Shell Source Convergence with Error

x/ε	10^{-3}	10^{-5}	10^{-7}	10^{-9}
1.00000E-02	7.61685E-02	7.61687E-02	7.61686E-02	7.61686E-02
5.64444E-01	8.66880E-02	8.66745E-02	8.66749E-02	8.66749E-02
1.11889E+00	9.93573E-02	9.94739E-02	9.94692E-02	9.94693E-02
1.67333E+00	3.06008E-02	3.06009E-02	3.06009E-02	3.06009E-02
2.22778E+00	1.55376E-02	1.55376E-02	1.55376E-02	1.55376E-02
2.78222E+00	9.31049E-03	9.31050E-03	9.31050E-03	9.31050E-03
3.33667E+00	6.11629E-03	6.11629E-03	6.11629E-03	6.11629E-03
3.89111E+00	4.26365E-03	4.26365E-03	4.26365E-03	4.26365E-03
4.44556E+00	3.09819E-03	3.09819E-03	3.09819E-03	3.09819E-03
5.00000E+00	2.32115E-03	2.32126E-03	2.32126E-03	2.32126E-03

Problem 5 considers the previous sample problem 1 for the shell source with the scalar flux given in Table 3. Again, complete convergence.

A second sample problem considers a comparison between all the 1D sources including the next source, the solid sphere. Figure 3 displays the results. The convergence of the three sources in spherical geometry is again evident at large distances from the source as expected.

3.2.4 Solid spherical source: NT/SP: I/LE/OG/I/L/X(C), A(C)/NFTI

Description

For this case, a solid spherical source of radius a emits isotropically in an infinite medium for $c = 0.9$, g=0.9 and $L = 20$.

Fig. 3. 1D Sources for H-G $g = 0.9$ $L = 20$ and $c = 0.9$

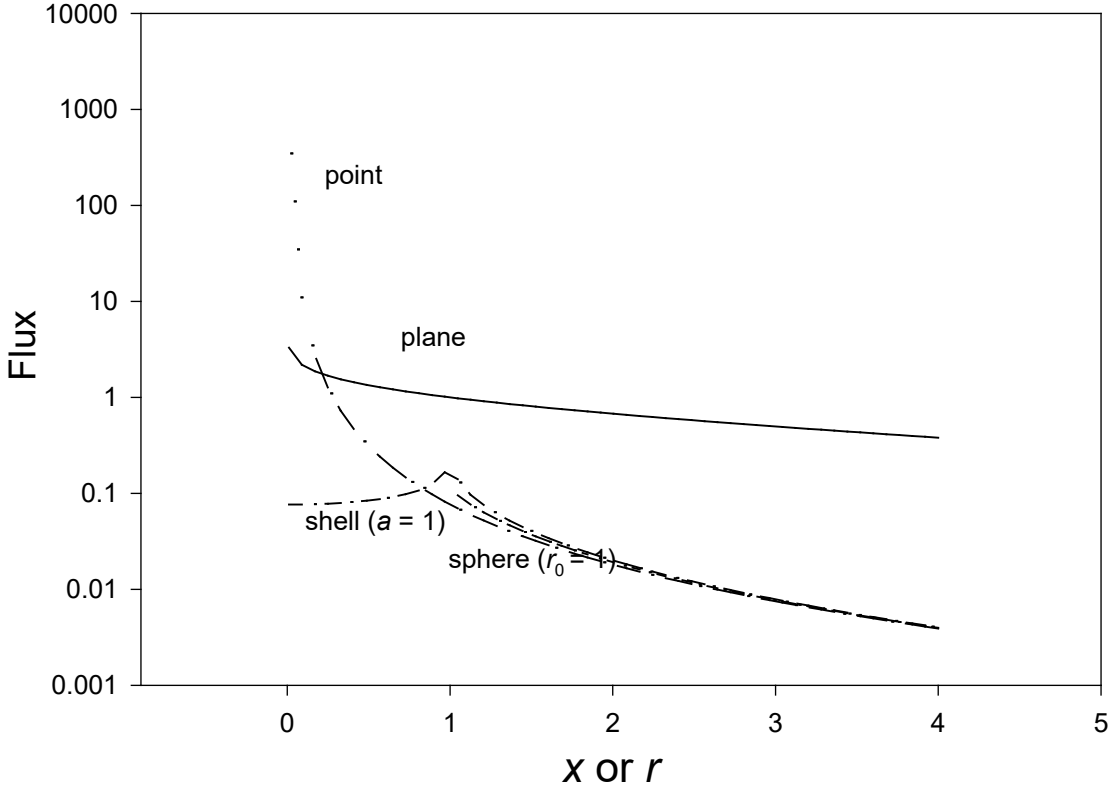

Theory

The flux from a spherical shell source of radius r_0 comes about by integration of the shell source over the spherical source volume

$$\Phi_{sp}(r) = q_0 \int_0^{r_0} da\ \Phi_{sh}(r,a). \tag{6}$$

When Eq(5) is substituted into this expression, there results

$$\Phi_{sp}(r) = \frac{1}{4\pi r_0^3} \int_{-r_0}^{r_0} da\ a\Phi_{pl}(|r-a|), \tag{7a}$$

with normalization

$$q_0 \equiv \frac{1}{4\pi r_0^3}, \tag{7b}$$

and a change of variable to simplify the integration. When we introduce Eq(A12) into Eq(7a) with the integration order interchanged,

the final expression for the shell source becomes

$$\Phi_{sp}(r)=\frac{1}{\pi}\int_{-\infty}^{\infty}dke^{ikr}\left\{z\frac{\tilde{g}_L(k)}{\Lambda_L(k)}\left[\frac{\sin(kr_0)}{k}-r_0\cos(kr_0)\right]\right\}. \quad (8)$$

Sample Problem 6

Table 4 presents the results for sample problem 6. This demonstration shows

Table 4. 1-D Sample Problem 6: Spherical Source for Two Integration Schemes
[H-G: g = 0.95, L = 20, c = 0.99]

x/ε	10^{-3}	10^{-5}	10^{-7}	$5x10^{-9}$	10^{-5}(AI)
1.0000E+00	1.2159E-01	1.2159E-01	1.2159E-01	1.2159E-01	**1.2157E-01**
1.1000E+00	8.6394E-02	8.6613E-02	8.6615E-02	8.6615E-02	**8.6611E-02**
1.2000E+00	6.8655E-02	6.8683E-02	6.8683E-02	6.8683E-02	**6.8683E-02**
1.3000E+00	5.6227E-02	5.6522E-02	5.6523E-02	5.6523E-02	**5.6522E-02**
1.4000E+00	4.7347E-02	4.7620E-02	4.7620E-02	4.7620E-02	**4.7620E-02**
1.5000E+00	4.0800E-02	4.0813E-02	4.0813E-02	4.0813E-02	**4.0813E-02**
1.6000E+00	3.5469E-02	3.5449E-02	3.5449E-02	3.5449E-02	**3.5449E-02**
1.7000E+00	3.1126E-02	3.1129E-02	3.1129E-02	3.1129E-02	**3.1129E-02**
1.8000E+00	2.7584E-02	2.7587E-02	2.7587E-02	2.7587E-02	**2.7587E-02**
1.9000E+00	2.4637E-02	2.4640E-02	2.4640E-02	2.4640E-02	**2.4640E-02**
2.0000E+00	2.2158E-02	2.2159E-02	2.2159E-02	2.2159E-02	**2.2159E-02**

the appropriateness of assisted integration (AI) (see section 5) versus direct integration for a spherical source of radius r_0 = 1. Five cases were run with the first four using direct integration and the last case (in bold) for assisted integration of the plane flux in Eq(7a) for error 10^{-5}. As observed, the direct and assisted integration schemes do indeed converge to the same values except near the source. AI provides an effective timesaving.

3.2.5 Finite Line Source: NT/CY: I/LE/OG/I/L/X(C), A(C)/NFTI

The advantage of the Fourier transform approach is that multidimensional sources are possible as now demonstrated in 2D.

Description

A finite vertical line source of length 2a emits isotropically in an infinite anisotropically scattering medium.

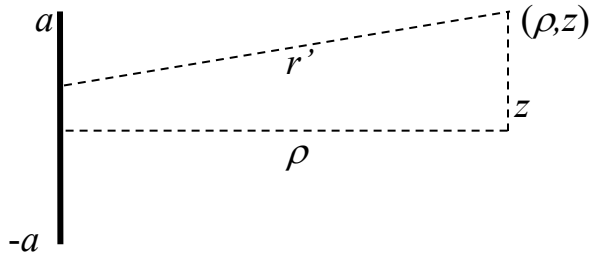

Theory

The flux at position (ρ, z) from the finite line source shown results from integration of the point source flux along the line source

$$\Phi_{2Dl}(\rho,z)=\int_{-a}^{a} dz'\Phi_{pt}(r'), \qquad (9)$$

which becomes, through a change of variable,

$$\Phi_{2Dl}(\rho,z)=\frac{1}{2}\int_{-1}^{1} d\omega\ \Phi_{pt}\left(\sqrt{\rho^2+(z-a\omega)^2}\right). \qquad (10)$$

For this case, the normalization is the inverse of the line source length. Unlike the 1D sources, an additional integration is required as indicated in Eq(10). The additional integration results from Gauss/Legendre quadrature to a high degree of accuracy as discussed below.

Sample Problem 7

Table 5 presents 2D results for Sample Problem 7-- a vertical line source of length 2 *mfp* with its center at the origin of an infinite medium. All digits quoted should be correct.

Table 5. Sample Problem 7: 2D Line Source

r\z	1.0000E+00	3.2500E+00	5.5000E+00	7.7500E+00	1.0000E+01
1.00000E-02	5.95091E-02	6.03556E-03	1.77000E-03	7.09800E-04	3.27906E-04
1.00750E+00	4.12872E-02	5.51407E-03	1.70119E-03	6.93411E-04	3.22674E-04
2.00500E+00	1.65815E-02	4.33449E-03	1.52071E-03	6.48108E-04	3.07868E-04
3.00250E+00	7.34388E-03	3.11436E-03	1.28132E-03	5.82093E-04	2.85323E-04
4.00000E+00	3.87014E-03	2.16158E-03	1.03454E-03	5.05436E-04	2.57545E-04

Figure 4 shows the longitudinal variation of the flux at various radial positions from the source.

Fig. 4. 2D Line Source [H-G: g = 0.9, L = 20, c = 0.9, a = 1.0]

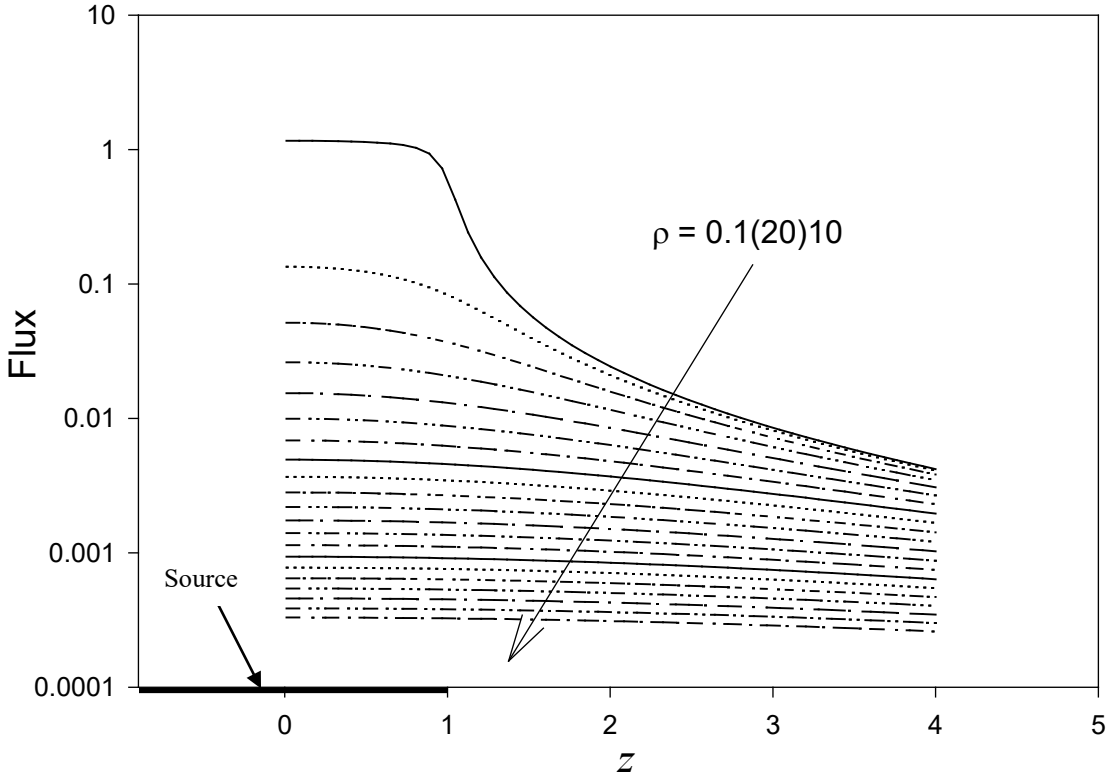

3.2.6 Ring source: NT/CY: I/LE/OG/I/L/X(C), A(C)/NFTI

Description

A circular source (ring) of radius a isotropically emits in an anisotropically scattering infinite medium. We are to find the radial and axial flux variation.

Theory

In a similar fashion, the flux from the circular source shown is determined

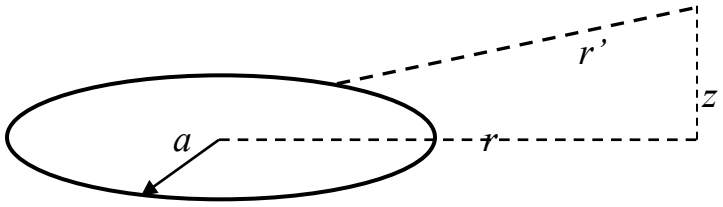

as

$$\Phi_{Cr}(\rho,z)=\frac{1}{\pi}\int_0^{\pi} d\theta\ \Phi_{pt}\left(\sqrt{z^2+a^2+r^2-2ar\cos(\theta)}\right), \qquad (11)$$

where the normalization

$$q_0 \equiv \frac{1}{2\pi a}$$

pertains. Again, the integration over the point source is numerical.

Sample Problem 8

The values in Table 6 give the scalar flux less the uncollided component for a ring source of radius r_0 = 1 and are seen to be highly precise. The parameters are g = 0.90, L = 20, c=0.9. Figure 5 shows the flux variation in

Table 6. Sample Problem (6.1): 2D Ring Source (r_0 = 1)

$r\backslash\varepsilon$	10^{-3}	10^{-5}	10^{-7}	10^{-9}
1.0000E-02	7.5491E-02	7.5491E-02	7.5491E-02	7.5491E-02
5.6444E-01	1.1004E-01	1.1003E-01	1.1003E-01	1.1003E-01
1.1189E+00	2.3759E-01	2.3759E-01	2.3759E-01	2.3759E-01
1.6733E+00	4.1353E-02	4.1353E-02	4.1353E-02	4.1353E-02
2.2278E+00	1.8205E-02	1.8205E-02	1.8205E-02	1.8205E-02
2.7822E+00	1.0295E-02	1.0295E-02	1.0295E-02	1.0295E-02
3.3367E+00	6.5650E-03	6.5650E-03	6.5650E-03	6.5650E-03
3.8911E+00	4.4969E-03	4.4969E-03	4.4969E-03	4.4969E-03
4.4456E+00	3.2310E-03	3.2311E-03	3.2311E-03	3.2311E-03
5.0000E+00	2.4023E-03	2.4023E-03	2.4023E-03	2.4023E-03

(r,z). The source position is evident as z approaches zero. As z moves further away from the source, the flux becomes uniform in the radial direction.

4. FUTURE DIRECTIONS

Several future directions will be considered in the future to provide a more comprehensive suite of infinite medium benchmarks. In particular, with the point source as a kernel, more complicated 3D geometrical source configurations are possible. In addition, a more efficient, less complicated, Fourier transform is envisioned to run faster than the current version. Finally, the implementation of a parallel version of the benchmarks will be a future focus.

Fig. 5 z-Variation for a Ring Source of $r_0 = 1$

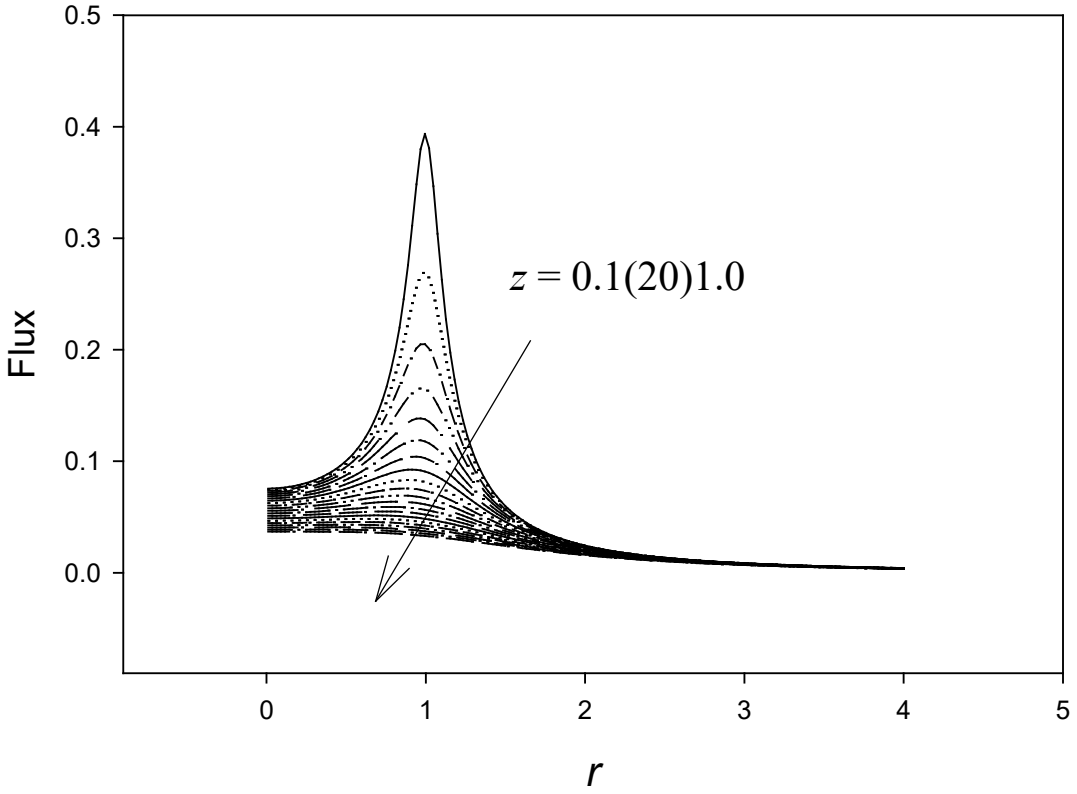

5. PROGRAMMING NOTES

5.1 Numerical Implementation

5.1.1 Assisted integration (AI) for 2-D sources

The assisted integrations referred to above use Gauss/Legendre (G/L) integration of order **Lm** shifted to the appropriate intervals. To expedite the integration and with an eye toward future accommodation of 3-D sources, an interpolation assisted (AI) integration scheme has been devised. Since these integrations involve only the plane or point flux, rather than evaluate this flux at all the integration abscissae, a simple interpolation scheme can be employed. This is possible because the integrand depends only on the relative distance from a point on the source to the point where the flux is to be determined. By predetermining the range of this distances (nearest to farthest) for all edit points, Φ_{pt} and Φ_{pl} are found at **nb** points in between. Thus, the desired integration abscissae come from (polynomial or rational) interpolation. This procedure greatly

reduces the computational effort but may not guarantee benchmark precision unless iteration on **nb** is required as we now discuss.

5.1.2 Iteration on quadrature order and interpolation abscissae

In order to guarantee benchmark quality, an outer iteration on the quadrature order (**Lm**) and the number of interpolation abscissae (**nb**) is performed. For simplicity, **Lm** and **nb** are set equal and the iteration counter then applies to both. These quantities are increased by two until the fluxes converge on the edit grid or the maximum number of iterations is reached. While benchmark accuracy (4- or 5- places) can be useful for 1D problems, most likely this will not be necessary for multi-dimensional comparisons since not more than three (or at most four digits) are expected from a multidimensional transport algorithm.

5.2 Code Operation

A Fortran 77 program called **tielv1.f** implements the numerical evaluation of the flux for the sources described above. **APPENDIX D** contains the program input and a sample problem. Multiple cases can be accommodated with output from 1D sources appropriate for (SigmaPlot™) plotting written to file **plt1.dat** and for 2D sources written to file **plt2.dat** (1D slices) or **plt3.dat** (3D mesh plot).

For best results and ease of use, the following considerations need to be taken into account when running **tielv1.f**:

1) The differential scattering cross section can be
   + read in from supplied file **wl.dat**
   + Henyey-Greenstein ($\omega_l = g^l$)
   + screened –Rutherford kernel
   + neutron elastic scattering kernel.

2) Because the integrands in Eqs(7a) and (10) become more singular on approach to either the line or circular sources, the integration will eventually fail. This breakdown occurs because the flux is infinite directly on either of these sources. For this reason, best results are obtained for edit points at least 0.05 *mfp* away from any source.

3) For multiple cases, all cases will have the same spatial edit grid.

4) The flux within a solid sphere is not determined and is set to zero.

5) Currently, the flux from a spherical source can be evaluated by both the direct (**isrc** = 4) and assisted (**isrc** = 41) integration schemes.

6. REFRENCES

[**Case,1967**], and P. Zweifel, *Linear Transport Theory*, Addison Wesley, MA, (1967).

[Ganapol,1991], INEL Report, EGG-NE-9641, 4/9, (1991).

[**Ganapol,1999a]**, J. Warsa, J. Dahl, S. Woolf and J. Garth, *Analytical Benchmark Comparisons for Matrix Eigenvalue-, Symbolic-, p-adaptive- and Standard- S_N Formulations*, ANS Math & Comp. Topical Meeting, Madrid, 1359(1999).

[**Ganapol,1999b]**, K. Parsons, *A Heterogeneous Medium Analytical Benchmark* , ANS Math & Comp. Topical Meeting, Madrid, 456(1999).

[Ganapol,2000], *A Consistent Theory of Neutral Particle Transport in an Infinite Medium*, TTSP, 43(2000).

[**Inonu,1973**], E. Inonu, *Jour. Math. Phys*., V11, 568(1973).

APPENDIX A
Theory for the Plane Source

The theory begins with the solution of the one-group transport equation in a plane infinite medium with isotropic source emission

$$\left[\mu\frac{\partial}{\partial x}+1\right]\Psi(x,\mu)=\frac{c}{2}\sum_{l=0}^{L}\omega_l P_l(\mu)\Psi_l(x)+\frac{\delta(x)}{2}. \qquad \text{(A1)}$$

$\Psi(x,\mu)$ represents the angular flux distribution of particles traveling in the direction μ (with respect to the x-axis) at the position x (measured in mean free paths from the source plane) and emitted by a source at $x = 0$. The Legendre moments of the scattering term in Eq(A1) are

$$\Psi_l(x)\equiv\int_{-1}^{1}d\mu P_l(\mu)\Psi(x,\mu)$$

and the particle flux distribution is to remain finite

$$\lim_{|x|\to\infty}\Psi(x,\mu)<\infty\ .$$

Note that any order of anisotropy L applies and the number of secondaries is c. If we operate on Eq(A1) by a Fourier transform, there results

$$(1+ik\mu)\bar{\Psi}(k,\mu)=\frac{c}{2}\sum_{l=0}^{L}\omega_l P_l(\mu)\bar{\Psi}(k)+\frac{1}{2}, \qquad \text{(A2)}$$

where the Fourier transform of the angular flux is

$$\bar{\Psi}(k,\mu)\equiv\int_{-\infty}^{\infty}dx\ e^{-ikx}\Psi(x,\mu);$$

and for the scalar flux

$$\bar{\Psi}(k)\equiv\int_{-\infty}^{\infty}dx\ e^{-ikx}\Psi(x).$$

The scalar flux solution, which is of primary interest, is therefore the inversion

$$\Psi(x)\equiv\frac{1}{2\pi}\int_{-\infty}^{\infty}dk\ e^{ikx}\bar{\Psi}_0(k).$$

Manipulation of Eq(A2) yields the following set of equations for the transformed moments $\bar{\Psi}_l$ [Ganapol,2000]:

$$\sum_{l=0}^{L}\left[\delta_{jl}-c\omega_l L_{jl}(k)\right]\bar{\Psi}_l(k)=(-1)^j\,zQ_j(z) \qquad \text{(A3)}$$

for $0\le j\le L$, where $z\equiv 1/ik$ and

$$L_{jl}(k)=\frac{1}{2}\int_{-1}^{1}d\mu\frac{P_j(\mu)P_l(\mu)}{1+ik\mu}.$$

$Q_j(z)$ is the j-th order Legendre function of the second kind. By projecting Eq(A2) over Legendre polynomials, a recurrence relation for the same transformed moments becomes

$$zh_l\bar{\Psi}_l(k)+(l+1)\bar{\Psi}_{l+1}(k)+l\bar{\Psi}_{l-1}(k)=z\delta_{l0} \qquad \text{(A4)}$$

with

$$h_l \equiv 2l+1-c\omega_l .$$

The set of equations most conveniently solved however, is neither Eq(A3) nor Eq(A4) alone but a combination of both, *i.e.*, Eq(A3) with $j = 0$ and Eq(A4) for $l = 0,\ldots L\text{-}1$.

The solution for the moments proceeds as follows. For convenience, define

$$\bar{\Psi}_l(k) \equiv \bar{\Psi}_l(-z)$$

to indicate the true dependence of $\bar{\Psi}_l(z)$. Equation (A4) becomes [Ganapol,2000]

$$-zh_l\bar{\Psi}_l(z)+(l+1)\bar{\Psi}_{l+1}(z)+l\bar{\Psi}_{l-1}(z)=-z\delta_{l0}, \qquad \text{(A5)}$$

and without loss of generality let its solution be of the form

$$\bar{\Psi}_l(z)=g_l(z)H(z)-\rho_l(z), \qquad \text{(A6)}$$

where g_l is the Chandrasekhar polynomial of the first kind that satisfies the homogeneous form of Eq(A5). H and ρ_l satisfy Eqs(A5) and (A3) for $j = 0$. Furthermore, if we impose the condition

$$H(z)=\bar{\Psi}_0(z),$$

then when with Eq(A6) introduced into Eq(A5), ρ_l must satisfy

$$-zh_l\rho_l(z)+(l+1)\rho_{l+1}(z)+l\rho_{l-1}(z)=0, \qquad \text{(A7)}$$

with starting value

$$\rho_0(z)\equiv 0 .$$

Equation (A7) defines the ρ_l- polynomials, called Chandrasekhar polynomials of the second kind [Inonu,1973]. We find $\bar{\Psi}_0(z)$ by substitution of Eq(A6) into Eq(A3) with $j = 0$

$$\bar{\Psi}_0(k)=\frac{\tilde{g}_L(k)}{\Lambda_L(k)}, \qquad \text{(A8a)}$$

where

$$\Lambda_L(k) = 1 - cz\sum_{l=0}^{L}\omega_l Q_l(z)\, g_l(z) \tag{A8b}$$

and

$$\tilde{g}_L(k) = \tilde{g}_L(z) \equiv zQ_0(z) - cz\sum_{l=0}^{L}\omega_l Q_l(z)\,\rho_l(z). \tag{A8c}$$

$\Lambda_L(z)$ is the usual dispersion relation for anisotropic scattering in terms of Chandrasekhar polynomials of the first kind. Once this connection has been identified, the simplifying relations of Inonu [Inonu,1973] give the remarkably compact representation

$$\Lambda_L(z) = (L+1)\left[g_{L+1}(z)Q_L(z) - g_L(z)Q_{L+1}(z)\right]. \tag{A9}$$

Apparently, the role of the ρ_l-polynomials is to define the numerator $\tilde{g}_L(k)$ of the zeroth moment transform. Following the same procedure (see **APPENDIX B**) as Inonu's, but for the ρ_l-polynomials, gives the corresponding condensed relation

$$\tilde{g}_L(z) = (L+1)\left[\rho_{L+1}(z)Q_L(z) - \rho_L(z)Q_{L+1}(z)\right] \tag{A10}$$

and Eq(A8a) becomes

$$\bar{\Psi}_0(k) = \left[\frac{\rho_{L+1}(z)Q_L(z) - \rho_L(z)Q_{L+1}(z)}{g_{L+1}(z)Q_L(z) - g_L(z)Q_{L+1}(z)}\right]. \tag{A11}$$

One obtains the scalar flux in plane geometry from the following Fourier transform inversion:

$$\Psi(x) \equiv \frac{1}{2\pi}\int_{-\infty}^{\infty} dk\; e^{ikx}\left[\frac{\tilde{g}_L(k)}{\Lambda_L(k)}\right]. \tag{A12}$$

This inversion can be evaluated either by analytical continuation of the integrand to pick up contributions from the poles (zeros of the dispersion relation) and branch cuts $\{[\pm i, \pm i\infty)\}$ or by numerical evaluation of the inversion integral directly. The latter is the evaluation of choice since it avoids determining the zeros of the dispersion explicitly, the number of which is unknown.

APPENDIX B
An Alternative Representation for $\tilde{g}_L(z)$

Following the procedure as outlined by Inonu [Inonu,1973], we begin with the recurrence relation for $\rho_j(z)$ for $j > 0$

$$-zh_j\rho_j(z)+(j+1)\rho_{j+1}(z)+j\,\rho_{j-1}(z)=0.$$

When this relation is multiplied by $Q_j(z)$ and summed from j=1 to L, there results

$$(L+1)\left[\rho_{L+1}(z)Q_L(z)-\rho_L(z)Q_{L+1}(z)\right]+$$
$$+\sum_{j=1}^{L}\rho_j(z)\left\{jQ_{j-1}(z)-(2j+1)zQ_j(z)+(j+1)Q_{j+1}(z)\right\}=zQ_0(z)-\omega z\sum_{j=0}^{L}\omega_j\rho_j(z)Q_j(z)\ .$$

The term in curly brackets vanishes since it is the recurrence relation for $Q_j(z)$ and the RHS is $\tilde{g}_L(z)$ giving the simplified expression by means of Inonu [Inonu,1973]

$$\tilde{g}_L(z)=zQ_0(z)-\omega z\sum_{l=0}^{L}\omega_l\rho_l(z)Q_l(z)$$
$$=(L+1)\left[\rho_{L+1}(z)Q_L(z)-\rho_L(z)Q_{L+1}(z)\right]\ . \qquad \text{(B1)}$$

APPENDIX C
Numerical Fourier Transform Inversion

The primary numerical procedure required for the numerical implementation of the six sources described above is the numerical Fourier transform inversion. This algorithm has been described in a previous report [Ganapol,1991] and therefore will not be described further other than to say it is an efficient and precise algorithm for the inversions of the image functions presented above.

Because of the singular nature of the flux from both the plane and point sources, the most appropriate representations of the solutions are

$$\Psi(x) \equiv \frac{1}{2} E_1(x) + \frac{1}{2\pi} \int_{-\infty}^{\infty} dk\ e^{ikx} \left[\frac{\tilde{g}_L(k)}{\Lambda_L(k)} - zQ_0(z) \right] \tag{C1}$$

$$\Phi_{pt}(r) \equiv \frac{e^{-r}}{4\pi r^2} + \frac{1}{2\pi} \int_{-\infty}^{\infty} dk\ e^{ikr} \left[\frac{\tilde{g}_L(k)}{z\Lambda_L(k)} - Q_0(z) \right] \tag{C2}$$

where the uncollided fluxes are explicitly found. Note that E_1 is the exponential integral of order one. In this way, the source singularities are isolated in the leading terms allowing the inversions to be determined more precisely.

APPENDIX D
Sample Problem Input and Output

The input description to **Tielv2.f** is given below. Also included are input

Table D.1
Input Description

```
c input description (file tielv1.dat)*********************************
c line 0 case identification
c
c line 1 ncc    number of cases
c        lmt    number of quadrature order iterations (10)
c
c line 2 nx     number of edit intervals between x0 and xl
c        x0     initial edit point
c        xl     final edit point
c
c note:if line 3 is not needed,enter one blank line
```



```
c line 3 mz     number of z edit points (for isrc=5,6 only)
c        z0     initial z edit point
c        zl     final z edit point
c
c note: repeat for each of the ncc cases
c line 4 iwl    1 read scattering coefficients (wl) from wl.dat file
c               2 Henyey-Greenstein (H-G) kernel
c               3 screened-Rutherford kernel
c               4 neutron elastic scattering
c        (note:if iwl<0 use transport correction)

c        ga     g for H-G and atomic mass for elastic neutron scattering
c        llmx   scattering order
c        w      number of secondaries
c        a0     shell,sphere radius or half line length
c        isrc   1  plane source
c               2  point source
c               3  shell source
c               4  spherical source (by direct inversion)
c               41 spherical source (by numerical integration)
c               5  line source
c               6  circular source
c        mb0    initial quadrature order (20)
c        err    desired relative error (1.0e-04)
c ****************************************************************
```

and output for a sample problem. The sample problem is for H-G scattering kernel with L = 10,15,20,35, g = 0.95, c = 0.9.

Table D.2
Sample Problem Input

```
sample problem
4 25                                  /ncc,lmt
10 0.01 4.0                          /nx,x0,xl
2 0.1 10.0                          /mx
2 0.95 10 0.9 1.0 3 20 1.0e-04 /iwl,ga,llmx,c,r0,isrc,mb,err
2 0.95 15 0.9 1.0 3 20 1.0e-04 /iwl,ga,llmx,c,r0,isrc,mb,err
2 0.95 20 0.9 1.0 3 20 1.0e-04 /iwl,ga,llmx,c,r0,isrc,mb,err
2 0.95 25 0.9 1.0 3 20 1.0e-04 /iwl,ga,llmx,c,r0,isrc,mb,err
```

Table D.3
Sample Problem Screen Output

```
begin case 1
 iwl    ga     llmx     w        a0     isrc mb     err
  2  9.500E-01  10  9.000E-01  1.000E+00   3  20  1.000E-04
quadrature order = 20 error=  0.000E+00
quadrature order = 22 error=  2.318E-03
quadrature order = 24 error=  5.881E-04
quadrature order = 26 error=  3.156E-04
quadrature order = 28 error=  3.626E-04
quadrature order = 30 error=  2.890E-04
quadrature order = 32 error=  1.594E-04
quadrature order = 34 error=  5.904E-05
begin case 2
  2  9.500E-01  15  9.000E-01  1.000E+00   3  20  1.000E-04
quadrature order = 20 error=  0.000E+00
quadrature order = 22 error=  2.326E-03
quadrature order = 24 error=  5.898E-04
quadrature order = 26 error=  3.160E-04
quadrature order = 28 error=  3.638E-04
quadrature order = 30 error=  2.900E-04
quadrature order = 32 error=  1.599E-04
quadrature order = 34 error=  5.924E-05
begin case 3
  2  9.500E-01  20  9.000E-01  1.000E+00   3  20  1.000E-04
quadrature order = 20 error=  0.000E+00
quadrature order = 22 error=  2.331E-03
quadrature order = 24 error=  5.911E-04
quadrature order = 26 error=  3.168E-04
quadrature order = 28 error=  3.646E-04
quadrature order = 30 error=  2.906E-04
quadrature order = 32 error=  1.602E-04
quadrature order = 34 error=  5.937E-05
begin case 4
  2  9.500E-01  25  9.000E-01  1.000E+00   3  20  1.000E-04
quadrature order = 20 error=  0.000E+00
quadrature order = 22 error=  2.327E-03
quadrature order = 24 error=  5.902E-04
quadrature order = 26 error=  3.163E-04
quadrature order = 28 error=  3.640E-04
```

---

quadrature order = 30 error= 2.902E-04
quadrature order = 32 error= 1.600E-04
quadrature order = 34 error= 5.928E-05

1-d Sources

x/case	1	2	3	4
error=	5.9044E-05	5.9237E-05	5.9368E-05	5.9281E-05
1.0000E-02,	7.3028E-02,	7.4198E-02,	7.4012E-02,	7.3992E-02,
4.0900E-01,	7.8143E-02,	7.9199E-02,	7.8923E-02,	7.8942E-02,
8.0800E-01,	1.0534E-01,	1.0500E-01,	1.0476E-01,	1.0492E-01,
1.2070E+00,	7.3614E-02,	7.3501E-02,	7.3331E-02,	7.3437E-02,
1.6060E+00,	3.2381E-02,	3.2708E-02,	3.2649E-02,	3.2652E-02,
2.0050E+00,	1.8808E-02,	1.8942E-02,	1.8942E-02,	1.8939E-02,
2.4040E+00,	1.2285E-02,	1.2322E-02,	1.2327E-02,	1.2326E-02,
2.8030E+00,	8.5925E-03,	8.5956E-03,	8.5984E-03,	8.5984E-03,
3.2020E+00,	6.2931E-03,	6.2870E-03,	6.2879E-03,	6.2880E-03,
3.6010E+00,	4.7667E-03,	4.7599E-03,	4.7600E-03,	4.7601E-03,
4.0000E+00,	3.7053E-03,	3.7001E-03,	3.7000E-03,	3.7000E-03,

plot file plt1.dat:1-D sources

time= 1.58227515

Revised 11.25.19